

The formation of $30M_{\odot}$ merging black holes at solar metallicity

Simone S. Bavera^{1,2,*}, Tassos Fragos^{1,2}, Emmanouil Zapartas³, Jeff J. Andrews^{4,5}, Vicky Kalogera⁵, Christopher P. L. Berry⁶, Matthias Kruckow^{1,2}, Aaron Dotter⁵, Konstantinos Kovelakas^{1,7,8}, Devina Misra¹, Kyle A. Rocha⁵, Philipp M. Srivastava^{5,9}, Meng Sun⁵, and Zepei Xing^{1,2}

¹Département d'Astronomie, Université de Genève, Chemin Pegasi 51, CH-1290 Versoix, Switzerland

²Gravitational Wave Science Center (GWSC), Université de Genève, CH-1211 Geneva, Switzerland

³IAASARS, National Observatory of Athens, Vas. Pavlou and I. Metaxa, Penteli, 15236, Greece

⁴Department of Physics, University of Florida, 2001 Museum Rd, Gainesville, FL 32611, USA

⁵Center for Interdisciplinary Exploration and Research in Astrophysics (CIERA) and Department of Physics and Astronomy, Northwestern University, 1800 Sherman Ave, Evanston, IL 60201, USA

⁶SUPA, School of Physics and Astronomy, University of Glasgow, Glasgow, G12 8QQ, UK

⁷Institute of Space Sciences (ICE, CSIC), Campus UAB, Carrer de Magrans, 08193 Barcelona, Spain

⁸Institut d'Estudis Espacials de Catalunya (IEEC), Carrer Gran Capità, 08034 Barcelona, Spain

⁹Electrical and Computer Engineering, Northwestern University, 2145 Sheridan Road, Evanston, IL 60208, USA

*e-mail: Simone.Bavera@unige.ch

ABSTRACT

The maximum mass of black holes formed in isolated binaries is determined by stellar winds and the interactions between the binary components. We consider for the first time fully self-consistent detailed stellar structure and binary evolution calculations in population-synthesis models and a new, qualitatively different picture emerges for the formation of black-hole binaries, compared to studies employing rapid population synthesis models. We find merging binary black holes can form with a non-negligible rate ($\sim 4 \times 10^{-7} M_{\odot}^{-1}$) at solar metallicity. Their progenitor stars with initial masses $\gtrsim 50M_{\odot}$ do not expand to supergiant radii, mostly avoiding significant dust-driven or luminous blue variable winds. Overall, the progenitor stars lose less mass in stellar winds, resulting in black holes as massive as $\sim 30M_{\odot}$, and, approximately half of them avoid a mass-transfer episode before forming the first-born black hole. Finally, binaries with initial periods of a few days, some of which may undergo episodes of Roche-lobe overflow mass transfer, result in mildly spinning first-born black holes, $\chi_{\text{BH1}} \lesssim 0.2$, assuming efficient angular-momentum transport.

Stellar-mass black holes (BHs) are known to populate our Universe. Evidence of their existence comes from X-ray binary (XRB) observations,^{1–3} gravitational-wave (GW) observations^{4–8} of coalescing binary BHs (BBHs), and, more recently, from joint radial velocity and astrometric observations.⁹ The inferred BH masses from XRBs and astrometric binaries cover the range from $4.5M_{\odot}$ to $21M_{\odot}$,^{2,9,10} while BHs observed through GWs the range from $2.6M_{\odot}$ to $106M_{\odot}$ ^{7,8} (assuming the lower-mass object in GW190814 is a BH). The dynamical measurement of BH masses in XRBs and astrometric binaries is possible only in the Milky Way and in nearby galaxies for XRBs,³ while current detections of GWs probe the Universe up to redshift $z \sim 1$.^{7,8} The discrepancy between the maximum BH mass inferred from XRBs and GWs has led to the belief that BHs with masses of around $30M_{\odot}$ can only originate from the evolution of massive stars born with sub-solar metallicities,^{4,11–14} namely below $Z_{\odot} = 0.0142$.¹⁵ This belief is anchored in the empirical evidence that stellar-wind mass-loss rates for massive stars scale with increasing metallicity.^{16–19} The maximum BH mass predicted by single stellar models depends on the mass loss of massive stars; however, this is uncertain due to the lack of observations of massive stars during their late evolutionary phases.^{20–24}

The stellar winds of massive stars, in addition to determining the final stellar mass, also affect stellar structure and the star's position in the Hertzsprung–Russell (HR) diagram.^{25,26} At solar metallicity, stellar winds of massive stars with zero-age main sequence (ZAMS) masses above $50M_{\odot}$ are so strong that they remove the hydrogen envelopes, exposing the cores of the stars. Unlike lower mass stars, these massive stars never expand to supergiant radii of $\sim 1000R_{\odot}$. Consequently, the feedback of wind mass loss onto stellar evolution makes the stellar tracks in the HR diagram turn to the blue before they become red supergiant stars. This established result of stellar evolution theory has been overlooked in models for the formation of merging BBHs. These models most often employ rapid binary population-synthesis (BPS) codes (e.g., BSE,²⁷ COSMIC,²⁸ COMPAS,²⁹ binary_c,^{30–32} MOBSE,³³ and StarTrack³⁴), where the impact of mass loss, either due to stellar winds or binary interactions, on the stellar properties is not treated self-consistently. Instead, the aforementioned BPS models employ

fitting formulae to precalculated single stellar evolutionary tracks, up to ZAMS masses of $50M_{\odot}$, at constant mass (SSE code^{35,36}). To model the evolution of the progenitors of stellar-mass BHs, these rapid BPS models extrapolate SSE stellar tracks up to $150M_{\odot}$. Mass loss due to stellar winds is applied a posteriori without accounting for the discussed mass loss feedback onto the stellar evolution. Rather, mass loss is implemented by interpolating a new stellar evolutionary track with the mass decreased by the mass lost through stellar winds in the given time-step, conserving the information of the stellar core of the original track.³⁵ The limitations of SSE stellar tracks in predicting the maximal radial expansion of massive stars at solar metallicity has been known since its conception.³⁵ However, less well studied is its impact on massive binary evolution and its implications for merging BBH formation, making it a major uncertainty in our current understanding.^{37,38} Although rapid BPS has been an invaluable tool in predicting and interpreting BBH and XRB observations thus far, advances in the simulations of binary stars^{39,40} allow us to revisit the topic.

Here, we use the POSYDON⁴⁰ framework which is a novel BPS that models self-consistently both stars and their binary interactions simultaneously. Other than accounting for the feedback of stellar wind mass loss onto the stellar evolution, POSYDON binary stellar models keep track in a detailed way the angular momentum transport within the stellar interiors of the binary components, and between the two binary components and the orbit. Additionally, POSYDON include self-consistent calculations of binary interactions and mass-transfer phases. To achieve this level of model sophistication, POSYDON uses pre-computed grids of detailed stellar structure and binary evolution simulations, performed with the MESA^{39,41–44} code, while at the same time maintaining the flexibility of rapid BPS codes. Other rapid BPS codes that rely on detailed models and, hence, not on SSE stellar tracks, do exist. For example, ComBiNE⁴⁵ and SEVEN¹² use look-up tables for the properties of single stars, based on grids of precalculated detailed, single-star models that take into account wind mass-loss self-consistently, while treating binary interactions using approximate prescriptions and parametrizations similar to the mentioned rapid BPS codes. Alternatively, BPASS⁴⁶ uses extensive grids of detailed binary evolution models computed with a custom version of the Cambridge STARS binary evolution code,⁴⁷ where both stars are followed in detail, but only one at a time for computational constraints. However, none of the aforementioned BPS codes, other than POSYDON, employ fully self-consistent detailed stellar-structure and binary simulations, including angular momentum transport in stellar interiors, which are essential to achieve accurate predictions of double compact object properties.

In this work, we examine how self-consistent modelling of mass loss, stellar structure, and binary interactions impacts the formation of merging BBHs at solar metallicity. First, we discuss BH formation in the context of single stellar evolution, focusing on the key aspects that determine the maximum BH mass. Second, we model the observational properties of merging BBHs in Milky-Way-like galaxies. In contrast to previous studies,^{48–50} our model predicts a non-negligible BBH merger rate at solar metallicity with BHs as massive as $\sim 30M_{\odot}$.

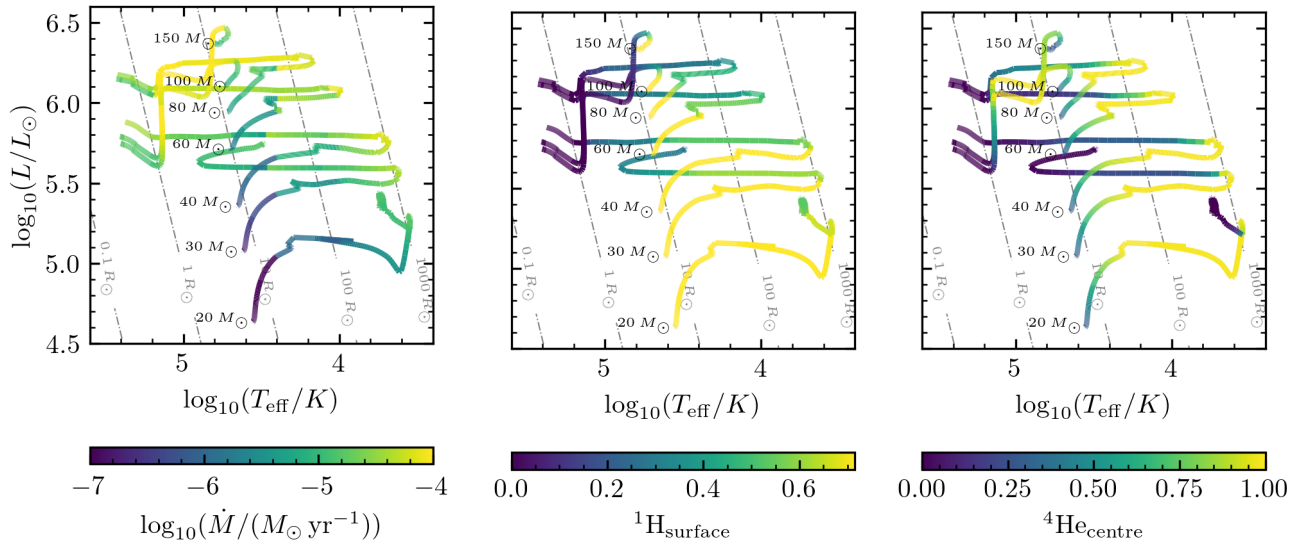


Figure 1. Hertzsprung–Russell diagram for stars with masses between $20M_{\odot}$ and $150M_{\odot}$. Stellar tracks are displayed up to central carbon depletion. The instantaneous mass loss (*left*), surface hydrogen abundance (*middle*) and centre helium abundance (*right*) are indicated by the track’s colour. Stars with masses $\gtrsim 80M_{\odot}$ reach the Wolf–Rayet phase while still burning hydrogen in their cores.

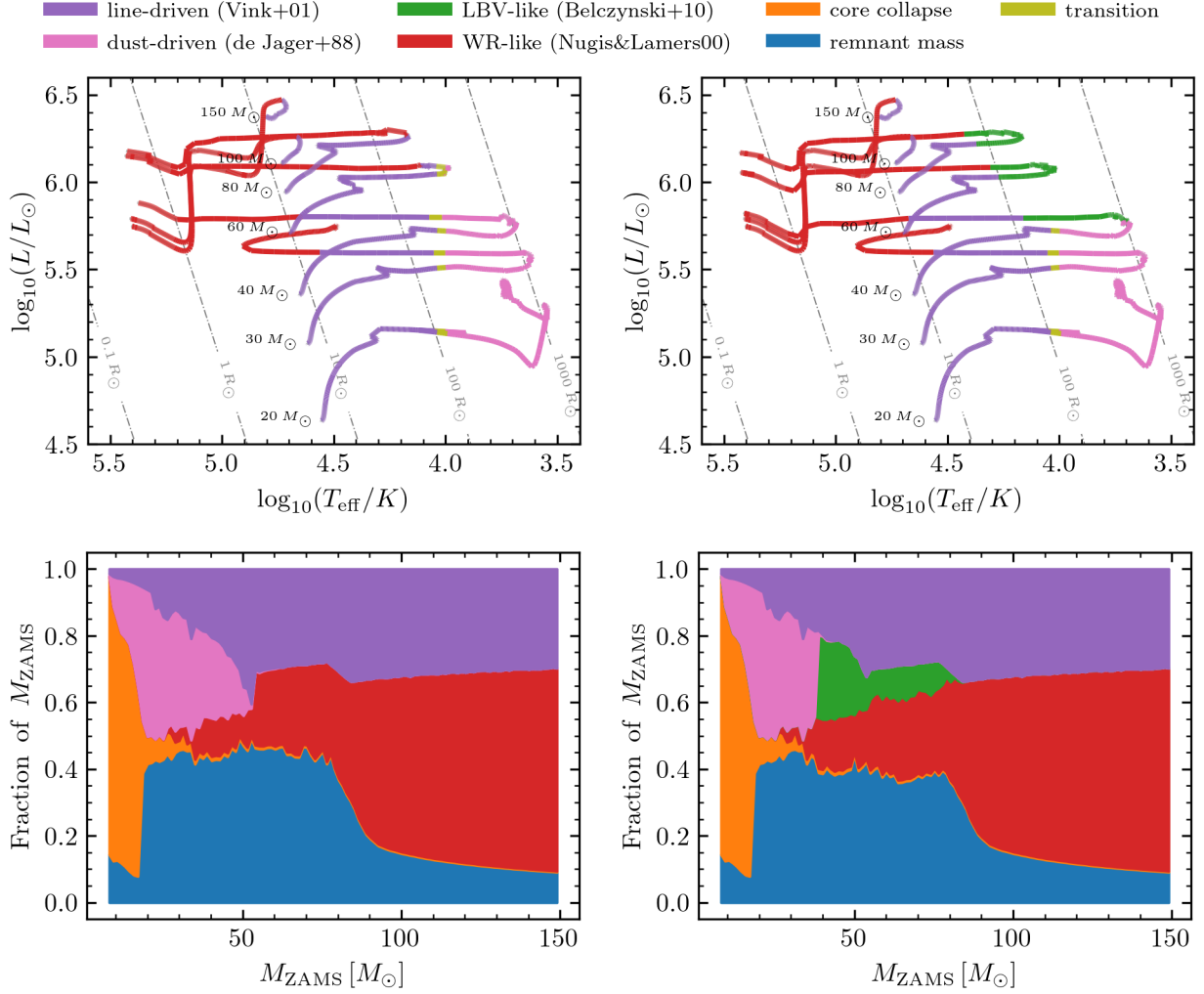


Figure 2. (Top) Hertzsprung–Russell diagram for stars with masses between $20M_{\odot}$ and $150M_{\odot}$. We denote with different colours indicating the different stellar wind prescriptions implemented in our default model (top-left) and model variation that includes LBV-like winds (top-right). (Bottom) Fraction of mass lost due to different mass loss mechanisms during the entire life of a POSYDON single star at solar metallicity as a function of ZAMS mass in the mass range between $8M_{\odot}$ and $150M_{\odot}$ sampled every $1.25M_{\odot}$. In our model, BH formation for single stars occurs for $M_{\text{ZAMS}} \gtrsim 17.3M_{\odot}$.

Results

The maximum BH mass from single stellar evolution at solar metallicity

We first present a subsample of the high-mass, single-star models at solar metallicity, and discuss their phenomenological evolution in the HR diagram. In Figure 1, we show stellar tracks in the mass range from $20M_{\odot}$ to $150M_{\odot}$, where we use a colour map to indicate the stellar-wind mass loss, as well as the surface ^1H and centre ^4He abundances of the stars during their evolution. Stars in this mass range are progenitors of stellar-mass BHs. In agreement with other state-of-the-art single-star models like GENEVA^{20,26,51,52} and MIST,⁵³ our stellar tracks of massive stars ($M_{\text{ZAMS}} \gtrsim 50M_{\odot}$) showed in Figure 1 expand less than those of lower-mass stars, after they leave the main sequence, and never reach the red supergiant phase where stars have radii of $\sim 1000R_{\odot}$. Stellar winds of the most massive stars ($\gtrsim 80M_{\odot}$) during the main sequence are so strong that deplete the hydrogen envelopes and induce the Wolf–Rayet (WR) phase while the stars are still burning hydrogen in their cores. Indeed, Figure 1 shows that the most massive stars reach the WR stage, i.e. when the surface ^1H fraction drops below 0.4 (see Methods), before the centre ^4He fraction becomes 1. Hence, these stars will experience a longer-lived WR phase and, consequently, experience most of their mass loss due to WR stellar winds. These stellar tracks result in final masses smaller than those of lower-mass stellar models. This distinct radial expansion signature of massive single stellar evolution at solar metallicity is not present when we consider a model variation without stellar-wind mass loss as the lack of such feedback onto stellar evolution

would cause the stars to expand to supergiant radii independently of their ZAMS mass (see Supplementary information).

Complementarily, the top-left panel of Figure 2 shows the different stellar-wind mass loss prescriptions applied to the tracks according to the fiducial (default) model of POSYDON (see Methods). POSYDON v1.0 default stellar models do not account for any luminous blue variable (LBV)-type winds. This choice was made given the uncertain estimates of LBV-type wind mass losses.⁵⁴ Regardless, here, we also consider a model variation of our default stellar assumptions which accounts for LBV-type winds when stars evolve above the Humphreys–Davidson limit (see Methods for further details). For comparison, the alternative model including LBV-type winds is shown in the top-right panel of Figure 2.

To illustrate how much mass is lost by the stars in the different stellar-wind regimes, in the bottom panels of Figure 2, we show the fraction of mass lost due to a given stellar wind prescription or core collapse with respect to the initial ZAMS mass. In both considered models, stars with $M_{\text{ZAMS}} \gtrsim 17.3 M_{\odot}$ may form a BH, given the assumed Patton&Sukhbold20⁵⁵ core-collapse prescription, where we also account for up to $0.5 M_{\odot}$ mass loss due to neutrinos in the core-collapse.⁴⁰ In contrast, less massive stars explode into a supernova to form a neutron star where a large fraction of the ZAMS mass is ejected in the process. The bottom panels of Figure 2 show that in both models, massive stars with $M_{\text{ZAMS}} \gtrsim 50 M_{\odot}$ lose most of their mass through WR winds.

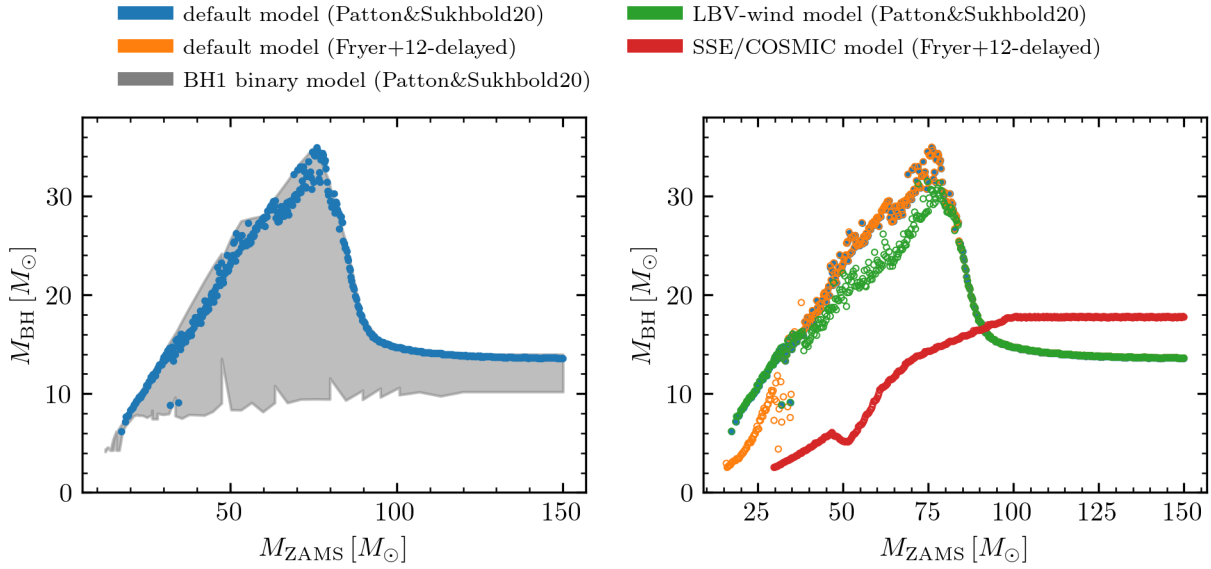


Figure 3. (Left) BH mass from single stellar evolution for a given ZAMS stellar mass at solar metallicity (markers) and the first-born BH mass of binary systems (gray area), with the extend of the grey area caused by the diversity of binary interactions starting at different orbital periods covered in POSYDON’s binary grids. (Right) We show the BH mass, resulting from single stars, given two different core-collapse assumptions for our default model according to the legend and the model variation including LBV-like winds. For comparison, we show BH masses as predicted by the SSE stellar models as implemented in COSMIC²⁸ given one of the considered core-collapse prescriptions.

To visualise the effect of wind mass loss of single stars onto the BH mass, in Figure 3, we show the BH mass as a function of ZAMS mass. The left panel of Figure 3, shows a nearly monotonic increasing relation between the stars ZAMS masses and the BH masses up to $M_{\text{ZAMS}} \simeq 80 M_{\odot}$. The maximum BH mass predicted by our default model is $\simeq 35.0 M_{\odot}$. In the same figure, for comparison, we also show the BH mass range corresponding to the formation of the first-born BH in the grid of binary-star models of POSYDON. The difference in the BH mass spectrum for a given ZAMS mass is caused by mass loss during binary mass transfer, which carries away some of the stellar mass prior to their core-collapse.

The right panel of Figure 3 shows the model variation accounting for LBV-type enhanced wind mass loss. This alternative model leads to slightly less massive BHs at solar metallicity with a maximum BH mass of $\simeq 31.5 M_{\odot}$. In the same figure, we also show a different assumption for the core-collapse, the Fryer+12-delayed⁵⁶ prescription, which is commonly used in rapid BPS studies. Both assumed core-collapse prescriptions predict direct collapse for stars with carbon–oxygen cores above $11 M_{\odot}$ at carbon depletion. Hence, in practice, both prescriptions predict the same BH masses for stars with $M_{\text{ZAMS}} \gtrsim 30 M_{\odot}$, while Fryer+12-delayed prescription predicts mass ejection for stars with $M_{\text{ZAMS}} \in [15.8, 30] M_{\odot}$, and, hence, less massive BHs. We also compare our model predictions with SSE stellar models. In the right panel of Figure 3, we show the BH masses as predicted by the Fryer+12-delayed prescription applied to SSE stellar models. In contrast to the POSYDON stellar models, SSE predicts much smaller BH masses for stars with $M_{\text{ZAMS}} \lesssim 90 M_{\odot}$ and a maximum BH mass of $\simeq 17.8 M_{\odot}$ for $M_{\text{ZAMS}} \gtrsim 90 M_{\odot}$,

noticeably smaller than the maximum BH mass predicted by POSYDON. The source of the difference originates from the overestimation of the radial expansion in SSE stellar tracks, which in turn shifts the fraction of the time that each track spends in the different stellar-wind regimes. In our models, we find that most of the stellar mass is lost by WR winds. By remaining more compact during their evolution, the BH progenitor stars avoid by the most part the regions of the HR diagram where dust-driven or LBV-type winds are expected to efficiently drive high mass-loss rates. In contrast, SSE predicts that massive stars ($M_{\text{ZAMS}} \gtrsim 50 M_{\odot}$) spend a considerable fraction of their evolution in the LBV-wind regime and lose most of their mass due to LBV-like winds (see the left panel of Figure 9 in Dorozzmai&Toonen22⁵⁷ which can be directly compared to our bottom panels of Figure 2). Correctly modeling the the maximal expansion of massive stars is crucial to accurately model merging BBHs and interpret GW observations.

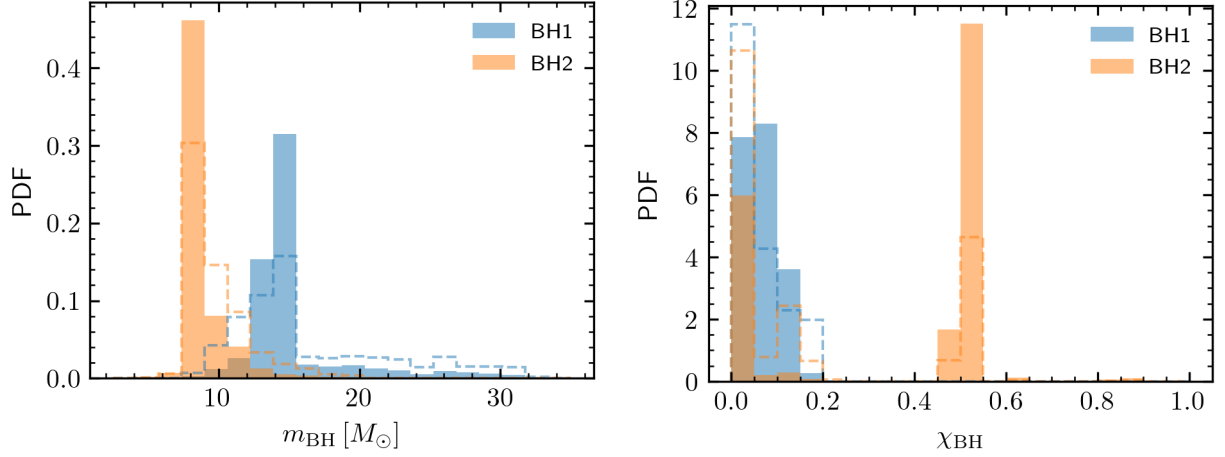


Figure 4. Merging binary black hole population at solar metallicity. Filled bins indicate the underlying (intrinsic) BBH distribution, while dashed lines illustrate selection effects for a ground-based GW detector. Here, we assume Advanced LIGO⁵⁸ at design sensitivity as an example. We distinguish with the indices 1,2 the first- and second-born BHs, respectively. (Left) BBH component mass distributions of merging BBHs formed from binary stars at solar metallicity. (Right) BBH component spin-magnitude distributions of merging BBHs formed from binary stars at solar metallicity. Systems with $\chi_{\text{BH}} > 0.4$ are believed to be associated with a luminous LGRB at the time of BH formation.⁵⁹

The population of merging BBHs at solar metallicity

The existence of massive BHs ($\simeq 30 M_{\odot}$) from single stars alone at solar metallicity does not directly imply that of similarly massive merging BBHs at solar metallicity. Compared to the progenitors of lower mass BHs, the progenitor stars of these massive BHs remain more compact during their evolution and avoid mass transfer before the formation of the first-born BH. For binary stars with primary ZAMS masses below $50 M_{\odot}$, Roche-lobe overflow occurs for systems with initial orbital periods of $\lesssim 10^{3.5}$ days, while for primaries with masses from $50 M_{\odot}$ to $80 M_{\odot}$ only for initial periods below the range $10^{1.8} - 10^{2.5}$ days depending on the binary mass ratio. Stars with birth masses of more than $80 M_{\odot}$ at solar metallicity can avoid mass transfer for initial periods down to a few days depending on the mass ratio (see Figure 6 in Supplementary information). Our POSYDON BPS model predicts the formation of merging BBH from both: (i) binaries that undergo a stable mass transfer prior to the formation of the first-born BH, and (ii) more massive binaries that avoid such phase. After the formation of the first-born BH, depending on the secondary mass, these systems will undergo a reverse stable mass-transfer^{60,61} or a common-envelope phase.^{13,62} In our BPS model at solar metallicity, all systems experiencing a common-envelope prior to the formation of the second-born BH avoid undergoing any mass transfer before the formation of the first-born BH.¹ In contrast, only one fourth of the systems undergoing a stable mass transfer prior to the formation of the second-born BH avoid undergoing any mass transfer before to the formation of the first-born BH. These alternative evolutionary pathways that avoid a stable mass-transfer episode before the formation of the first-born BH stand in contrast to what commonly found with rapid BPS models at sub-solar metallicity where such phase is present.^{63,64}

In the left panel of Figure 4, we show the component BH mass distribution of the intrinsic merging BBH population at solar metallicity. The distribution is constructed by distributing the synthetic BBH population obtained from the BPS model following

¹In our results, we exclude binaries that experience reverse mass-transfer prior to the formation of the first-born BH. This is due to these systems not being treated properly by MESA in the version used in POSYDON v1.0. This problem affects approximately 4% of tracks in the grid of binaries consisting of two hydrogen-rich main-sequence stars (see Section 5.5 of the POSYDON instrument paper⁴⁰).

the star formation history of the Universe consistent with the stars having solar metallicity. Specifically, to obtain the underlying merging BBH population at solar metallicity, we use the *IllustrisTNG*⁶⁵ simulated star formation rate happening in the metallicity range $[0.5Z_{\odot}, 2Z_{\odot}]$. For comparison, in Figure 4 we also indicate a similar distribution that accounts for selection effects of a ground-based GW detector. As an example, we consider Advanced LIGO⁵⁸ at design sensitivity⁶⁶ (see the Methods section for further details). We find that the BH mass spectrum of merging BBHs at solar metallicity spans the same range of BH masses formed from single stars. However, we find fewer BHs above $16M_{\odot}$. We quantify the fraction of first-born BHs with masses above $20M_{\odot}$ to be $f_{m_{\text{BH1}} > 20M_{\odot}} = 0.10$, while those of above $30M_{\odot}$ constitute a fraction of $f_{m_{\text{BH1}} > 30M_{\odot}} = 0.01$. When accounting for LIGO selection effects, these fractions increase to $f_{m_{\text{BH1}} > 20M_{\odot}}^{\text{det}} = 0.24$ and $f_{m_{\text{BH1}} > 30M_{\odot}}^{\text{det}} = 0.03$, respectively. These results cannot be compared directly to the observed sample of BBHs from the LIGO Scientific, Virgo and KAGRA Collaboration,^{5–8} as observed merging BBHs come from a range of metallicities. One would expect that accounting for the lower metallicity stellar populations would increase the average BH mass, in which case the aforementioned fractions can be interpreted as lower limits when compared to the total observed population.

Furthermore, in contrast to past studies,^{48–50} we find a non-negligible BBH merger rate efficiency per stellar mass formation of $4.4 \times 10^{-7} M_{\odot}^{-1}$ at solar metallicity. Of the total rate, around 40% comes from systems undergoing a common-envelope phase, around 45% undergo a stable mass-transfer phase before the formation of each BH, and around 15% experience a stable mass-transfer phase only after the formation of the first-born BH. Accounting again only for the Universe star formation rate in the metallicity range $[0.5Z_{\odot}, 2Z_{\odot}]$, we can estimate the intrinsic local merger rate density of BBHs formed at solar metallicity to $8.6 \text{ Gpc}^{-3} \text{ yr}^{-1}$ and the corresponding detection rate for Advanced LIGO at design sensitivity to around 25 yr^{-1} . Again, these rates are not to be directly compared to the ones inferred from the LIGO Scientific, Virgo and KAGRA Collaboration⁶⁷ due to the omission in our models of the BBH population formed at low-metallicity environments. Nevertheless, should our predicted rates be higher than the observed ones, our model would be inconsistent with observations.

In the right panel of Figure 4, we show the component BH dimensionless spin parameters of the modeled merging BBH population at solar metallicity. Our BPS model predicts an underlying fraction of 19% of merging BBHs with first-born BH spins in the range $0.1 \leq \chi_{\text{BH1}} \leq 0.2$. The progenitor stars of these mildly spinning BHs have masses $M_{\text{ZAMS}} > 50M_{\odot}$ and orbits with initial periods of a few days. They may undergo episodes of Case-A Roche-lobe overflow mass-transfer or stable contact phase, which limits the expansion of the orbit, or in some cases avoid mass-transfer all together. In all cases, the two stars remain sufficiently close to each other where tides can maintain the primary star rotating until the formation of a mildly-spinning first-born BHs when efficient angular momentum transport is assumed (see Figure 6 in Supplementary information). This result is opposed to the common assumption in recent rapid BPS studies^{63,64,68,69} that efficient angular momentum transport leads to the formation of first-born BHs with negligible spin.

The spin of the second-born BH is determined by the tidal interactions during the BH–WR phase. In agreement with past studies, we find that only systems evolving through a common envelope reach a close enough orbital separation to experience significant tidal spin-up.⁷⁰ The formation of BHs with high spins of $\chi_{\text{BH}} > 0.4$ has been associated with luminous LGRBs at the formation of the BH.⁵⁹ Our prediction for the formation of BHs with $\chi_{\text{BH}} > 0.4$ at solar metallicity and hence existence of LGRBs at solar metallicity (in contrast to earlier work by Bavera+22⁵⁹ based partly on rapid BPS calculations) is consistent with the solar-like inferred metallicities of a small fraction of LGRB host galaxies.⁷¹

The results presented in this section are a direct consequence of the reduced maximal expansion of massive stars at solar metallicity. Previously mentioned rapid BPS codes based on detailed stellar models, i.e. not SSE stellar tracks, do share similar trends. For example, *SEVN* models^{12,72,73} also predicts the formation of massive BHs at solar metallicity and a similar non-negligible BBH merger rate efficiency per solar mass. In contrast, *ComBiNE* models^{45,74} predict a smaller maximal BH mass than the one predicted here. This is because these models assume stronger WR winds and less fall back mass during BH formation compared to our fiducial assumptions. *BPASS* models^{46,75} predict BH masses of a few solar masses greater than rapid BPS codes employing the SSE stellar tracks at solar metallicity but a lower BBH merger rates compared to the one presented here. However, none of the aforementioned BPS models other than *POSDON* employing fully self-consistent detailed stellar-structure and binary simulations can accurately predict merging BBH spin distributions, which have been shown to be crucial for differentiating BBHs formed via isolated binary evolution as opposed to other formation channels.⁷⁶

Discussion & Conclusions

The existence of massive, $\sim 30M_{\odot}$, BHs formed from stars born at solar metallicity has multiple observational implications for binary systems in the context of GW detections, XRBs and astrometric binaries. These massive BHs have been observed since the first detection of GWs, GW150914,⁴ which were previously interpreted to have originated from the evolution of sub-solar metallicity stars.¹⁴ Such conclusions were based on rapid BPS models of BBH formation which, in contrast to the models presented here, do not predict such massive merging BBHs at solar metallicity as these models overpredict the expansions and consequently the mass loss of massive stars ($\gtrsim 50M_{\odot}$). One would also expect that the predicted existence of such massive BHs at solar metallicity would imply their potential observability in XRBs.⁷⁷ If confirmed, a potential candidate of such massive BH

is the one harboured in the galactic XRB MAXI J1631-479 with its updated mass estimate in the range of $15 M_{\odot}$ to $45 M_{\odot}$.⁷⁸ Alternatively, future astrometric observations of detached wide binaries in the Milky Way^{9,79,80} and globular clusters^{81,82} will be another potential tool to indirectly observe these massive BHs.^{83,84} The discovery of these massive BHs in binary systems at solar metallicity will be a new probe into the evolution of massive stars. Such discovery, built upon model predictions made here, has the potential to broadly impact astrophysics, from our theoretical understanding of galaxy evolution to the formation of heavy elements.

This study investigated BH formation from single and binary evolution at solar metallicity. In contrast to commonly used stellar models in rapid BPS, we showed that stellar binary models that self-consistently account for the feedback of stellar wind mass loss and binary interactions onto stellar evolution lead to the formation of more massive merging BHs than previously thought. Our fiducial POSYDON single stellar model predicts that massive stars ($M_{\text{ZAMS}} \gtrsim 50 M_{\odot}$) do not expand to red supergiant radii but rather remain more compact. Additionally, stars with ZAMS masses above $80 M_{\odot}$ reach the WR phase while still burning hydrogen in their cores. These massive stars will experience a longer WR phase compared to lower mass stars, forming lower mass BHs and setting the maximum BH mass at solar metallicity at $\simeq 35 M_{\odot}$ ($\simeq 31.5 M_{\odot}$ when accounting for LBV-type winds). Even though our model of single stellar evolution predicts the existence of massive BHs at solar metallicity, our BPS model predicts a challenging to discover intrinsic fraction ($\sim 1\%$) of merging BBHs with masses above $30 M_{\odot}$. When accounting for the LIGO’s detectors selection effects at design sensitivity the fraction of massive BHs above $30 M_{\odot}$ at solar metallicity increases to $\sim 3\%$ for around one detection per year from binaries in the metallicity range $[0.5Z_{\odot}, 2Z_{\odot}]$. Finally, we find that binaries with primary stars of initial mass $M_{\text{ZAMS}} \gtrsim 50 M_{\odot}$ and initial period of a few days may undergo episodes of Case-A Roche-lobe overflow mass-transfer, a stable contact phase or avoid mass transfer at all, keeping their orbit close and result to mildly spinning first-born BHs ($\chi_{\text{BH1}} \lesssim 0.2$) when efficient angular momentum transport is assumed. This predicted BH spin signature is in agreement with the analysis of the observed population of merging BBHs.⁸⁵

Our results demonstrate the importance of the self-consistent modeling of mass loss in BPS models, which have been shown here to be crucial for the interpretation of the origin GW sources, XRBs and astrometric BHs.

Methods

Single stellar models

In this study, we generate a grid of MESA^{39,41–44} single star simulations with ZAMS masses in the range $[8, 150] M_{\odot}$ with resolution $\Delta M_{\text{ZAMS}} = 0.25 M_{\odot}$. Our default model follows the stellar model assumptions of POSYDON.⁴⁰ The assumed wind mass loss scheme is known as the *Dutch wind scheme* and includes: the Vink+01¹⁶ line-driven winds for stars with effective temperatures above 11,000 K, a linear transition phase to the de Jager+88¹⁸ dust-driven winds for cooler stars with effective temperatures below 10,000 K, and Nugis&Lamers00¹⁹ winds for WR stars defined as having effective temperatures above 11,000 K when the surface ^1H abundance is below the value 0.4.

The default POSYDON stellar model assumes there is no LBV-like wind enhanced mass loss when stars evolve through the Humphreys–Davidson limit.⁸⁶ This choice was made given the uncertain estimates of LBV-type wind mass losses.⁵⁴ To verify how our results depend on the assumed lack of LBV-type wind, we consider a model variation including LBV-like winds following Belczynski+10.¹¹ In practice, the wind mass loss during the LBV-wind phase (shown in the top-right panel of Figure 2) is enhanced to $10^{-4} M_{\odot} \text{yr}^{-1}$ for stars with both $L > 6 \times 10^5 L_{\odot}$ and $R/R_{\odot} (L/L_{\odot})^{1/2} > 10^5$ compared to default model shown in the left plot of Figure 1. Additionally, to illustrate the significance of winds to the evolution of massive stars ($M_{\text{ZAMS}} \geq 50 M_{\odot}$), we consider an additional model variation where no stellar-wind mass loss are implemented. This alternative model, presented in the Supplementary information, shows that neglecting the feedback of mass loss into stellar evolution leads to the expansion of stars to supergiant radii independently from their initial mass.

The stellar-evolution models are stopped when core carbon is depleted, after which we assume their collapse is imminent. We evaluate the core-collapse of the massive stars into BHs following the Patton&Sukhbold22⁵⁵ N20 engine prescription, as implemented in POSYDON.⁴⁰ To verify how our results depend on the assumed core-collapse prescription, we also consider the commonly used Fryer+12⁵⁶ Delayed prescription, from now on referred to as (Fryer+12-delayed), as implemented in POSYDON.⁴⁰

Binary population synthesis model

We use the POSYDON framework, to generate a BBH population-synthesis model based on grids of detailed MESA stellar structure and binary evolution simulations (revision 11701). We simulated a total of 50 million massive binary systems following the default assumptions made in POSYDON v1.0 instrument paper.⁴⁰ This set of default assumptions is not the result of specific model calibration. Rather, model assumptions were made, given our best current theoretical and observational understanding of stellar and binary physics processes. POSYDON generates a synthetic catalog of merging BBHs at solar metallicity. To obtain the underlying (intrinsic) population of merging BBHs at solar metallicity in the Universe, we convolve the synthetic population with the IllustrisTNG⁶⁵ star formation rate (SFR) as implemented in Bavera+.^{59,63,64} As our

population-synthesis model is evaluated at solar metallicity, we only account for the SFR in the metallicity range $[0.5Z_{\odot}, 2Z_{\odot}]$. To obtain the detectable BBH population observed by Advanced LIGO⁵⁸ at design sensitivity,⁶⁶ we account for the selection effects of the GW detector following the methodology and implementation of Barrett+18.⁸⁷ In practice, we compute the detection probability of a merging BBH system given the BH mass components and the redshift of merger. Here, we ignored the impact of BH spin on detectability as our intrinsic merging BBH population is dominated by slowly spinning BHs and the impact of BH spins on detectability is minor compared to the BH mass selection effects.⁸⁸ The optimal signal-to-noise ratio for a face-on source is computed for a single detector using the sensitivity above with GW waveforms from `lalsuite`.⁸⁹ The optimal signal-to-noise ratio is then convolved with the antenna pattern function distribution,⁹⁰ which allows us to estimate the probability of detection. In our model we assume that signals are detected if their single-detector signal-to-noise ratio threshold exceeds a threshold value of 8.⁹¹

Acknowledgements

This work was supported by the Swiss National Science Foundation Professorship grant (project numbers PP00P2_176868 and PP00P2_211006). The `POSYDON` project is supported primarily by two sources: a Swiss National Science Foundation Professorship grant (PI Fragos, project number PP00P2_176868) and the Gordon and Betty Moore Foundation (PI Kalogera, grant award GBMF8477). CPLB acknowledges support from the University of Glasgow. KK acknowledges support from the Federal Commission for Scholarships for Foreign Students for the Swiss Government Excellence Scholarship (ESKAS No. 2021.0277), and the Spanish State Research Agency, through the María de Maeztu Program for Centers and Units of Excellence in R&D, No. CEX2020-001058-M. K.A.R. also thanks the LSSTC Data Science Fellowship Program, which is funded by LSSTC, NSF Cybertraining Grant No. 1829740, the Brinson Foundation, and the Moore Foundation; their participation in the program has benefited this work. All figures were made with the open-source Python module `Matplotlib`.⁹² This research used the Python modules `Astropy`,⁹³ `iPython`,⁹⁴ `Numpy`,⁹⁵ `Pandas`,⁹⁶ and `SciPy`.⁹⁷

Authors contributions

All authors contributed to the work presented in this paper. SSB lead the writing with substantial contributions of TF, EZ, JJA, VK, CPLB, and MK. The results presented in this study were obtained using the open-source software `POSYDON`, which was developed by SSB, TF, JJA, EZ, AD, KK, DM, KAR, PMS, MS and ZX.

Competing interests

The authors declare no competing interests.

References

1. Remillard, R. A. & McClintock, J. E. X-Ray Properties of Black-Hole Binaries. *Annu. Rev. Astron. Astrophys.* **44**, 49–92, DOI: [10.1146/annurev.astro.44.051905.092532](https://doi.org/10.1146/annurev.astro.44.051905.092532) (2006). [astro-ph/0606352](https://arxiv.org/abs/astro-ph/0606352).
2. Corral-Santana, J. M. *et al.* BlackCAT: A catalogue of stellar-mass black holes in X-ray transients. *Astron. Astrophys.* **587**, A61, DOI: [10.1051/0004-6361/201527130](https://doi.org/10.1051/0004-6361/201527130) (2016). [1510.08869](https://arxiv.org/abs/1510.08869).
3. Tetarenko, B. E., Sivakoff, G. R., Heinke, C. O. & Gladstone, J. C. WATCHDOG: A Comprehensive All-sky Database of Galactic Black Hole X-ray Binaries. *Astrophys. J. Suppl. Ser.* **222**, 15, DOI: [10.3847/0067-0049/222/2/15](https://doi.org/10.3847/0067-0049/222/2/15) (2016). [1512.00778](https://arxiv.org/abs/1512.00778).
4. Abbott, B. P. *et al.* Observation of Gravitational Waves from a Binary Black Hole Merger. *Phys. Rev. Lett.* **116**, 061102, DOI: [10.1103/PhysRevLett.116.061102](https://doi.org/10.1103/PhysRevLett.116.061102) (2016). [1602.03837](https://arxiv.org/abs/1602.03837).
5. Abbott, B. P. *et al.* GWTC-1: A Gravitational-Wave Transient Catalog of Compact Binary Mergers Observed by LIGO and Virgo during the First and Second Observing Runs. *Phys. Rev. X* **9**, 031040, DOI: [10.1103/PhysRevX.9.031040](https://doi.org/10.1103/PhysRevX.9.031040) (2019). [1811.12907](https://arxiv.org/abs/1811.12907).
6. Abbott, R. *et al.* GWTC-2: Compact Binary Coalescences Observed by LIGO and Virgo during the First Half of the Third Observing Run. *Phys. Rev. X* **11**, 021053, DOI: [10.1103/PhysRevX.11.021053](https://doi.org/10.1103/PhysRevX.11.021053) (2021). [2010.14527](https://arxiv.org/abs/2010.14527).
7. Abbott, R. *et al.* GWTC-2.1: Deep Extended Catalog of Compact Binary Coalescences Observed by LIGO and Virgo During the First Half of the Third Observing Run. *arXiv e-prints* arXiv:2108.01045 (2021). [2108.01045](https://arxiv.org/abs/2108.01045).
8. Abbott, R. *et al.* GWTC-3: Compact Binary Coalescences Observed by LIGO and Virgo During the Second Part of the Third Observing Run. *arXiv e-prints* arXiv:2111.03606 (2021). [2111.03606](https://arxiv.org/abs/2111.03606).

9. El-Badry, K. *et al.* A Sun-like star orbiting a black hole. *Mon. Not. R. Astron. Soc.* **518**, 1057–1085, DOI: [10.1093/mnras/stac3140](https://doi.org/10.1093/mnras/stac3140) (2023). [2209.06833](https://arxiv.org/abs/2209.06833).
10. Miller-Jones, J. C. A. *et al.* Cygnus X-1 contains a 21-solar mass black hole—Implications for massive star winds. *Science* **371**, 1046–1049, DOI: [10.1126/science.abb3363](https://doi.org/10.1126/science.abb3363) (2021). [2102.09091](https://arxiv.org/abs/2102.09091).
11. Belczynski, K. *et al.* On the Maximum Mass of Stellar Black Holes. *Astrophys. J.* **714**, 1217–1226, DOI: [10.1088/0004-637X/714/2/1217](https://doi.org/10.1088/0004-637X/714/2/1217) (2010). [0904.2784](https://arxiv.org/abs/0904.2784).
12. Spera, M., Mapelli, M. & Bressan, A. The mass spectrum of compact remnants from the PARSEC stellar evolution tracks. *Mon. Not. R. Astron. Soc.* **451**, 4086–4103, DOI: [10.1093/mnras/stv1161](https://doi.org/10.1093/mnras/stv1161) (2015). [1505.05201](https://arxiv.org/abs/1505.05201).
13. Belczynski, K., Holz, D. E., Bulik, T. & O’Shaughnessy, R. The first gravitational-wave source from the isolated evolution of two stars in the 40–100 solar mass range. *Nature* **534**, 512–515, DOI: [10.1038/nature18322](https://doi.org/10.1038/nature18322) (2016). [1602.04531](https://arxiv.org/abs/1602.04531).
14. Abbott, B. P. *et al.* Astrophysical Implications of the Binary Black-hole Merger GW150914. *Astrophys. J. Lett.* **818**, L22, DOI: [10.3847/2041-8205/818/2/L22](https://doi.org/10.3847/2041-8205/818/2/L22) (2016). [1602.03846](https://arxiv.org/abs/1602.03846).
15. Asplund, M., Grevesse, N., Sauval, A. J. & Scott, P. The Chemical Composition of the Sun. *Annu. Rev. Astron. Astrophys.* **47**, 481–522, DOI: [10.1146/annurev.astro.46.060407.145222](https://doi.org/10.1146/annurev.astro.46.060407.145222) (2009). [0909.0948](https://arxiv.org/abs/0909.0948).
16. Vink, J. S., de Koter, A. & Lamers, H. J. G. L. M. Mass-loss predictions for O and B stars as a function of metallicity. *Astron. Astrophys.* **369**, 574–588, DOI: [10.1051/0004-6361:20010127](https://doi.org/10.1051/0004-6361:20010127) (2001). [astro-ph/0101509](https://arxiv.org/abs/astro-ph/0101509).
17. Vink, J. S. & Sander, A. A. C. Metallicity-dependent wind parameter predictions for OB stars. *Mon. Not. R. Astron. Soc.* **504**, 2051–2061, DOI: [10.1093/mnras/stab902](https://doi.org/10.1093/mnras/stab902) (2021). [2103.12736](https://arxiv.org/abs/2103.12736).
18. de Jager, C., Nieuwenhuijzen, H. & van der Hucht, K. A. Mass loss rates in the Hertzsprung-Russell diagram. *Astron. Astrophys. Suppl.* **72**, 259–289 (1988).
19. Nugis, T. & Lamers, H. J. G. L. M. Mass-loss rates of Wolf-Rayet stars as a function of stellar parameters. *Astron. Astrophys.* **360**, 227–244 (2000).
20. Meynet, G., Maeder, A., Schaller, G., Schaerer, D. & Charbonnel, C. Grids of massive stars with high mass loss rates. V. From 12 to 120 M_{\odot} at $Z=0.001, 0.004, 0.008, 0.020$ and 0.040 . *Astron. Astrophys. Suppl.* **103**, 97–105 (1994).
21. Smith, N. Mass Loss: Its Effect on the Evolution and Fate of High-Mass Stars. *Annu. Rev. Astron. Astrophys.* **52**, 487–528, DOI: [10.1146/annurev-astro-081913-040025](https://doi.org/10.1146/annurev-astro-081913-040025) (2014). [1402.1237](https://arxiv.org/abs/1402.1237).
22. Renzo, M., Ott, C. D., Shore, S. N. & de Mink, S. E. Systematic survey of the effects of wind mass loss algorithms on the evolution of single massive stars. *Astron. Astrophys.* **603**, A118, DOI: [10.1051/0004-6361/201730698](https://doi.org/10.1051/0004-6361/201730698) (2017). [1703.09705](https://arxiv.org/abs/1703.09705).
23. Belczynski, K. *et al.* The Formation of a 70 M_{\odot} Black Hole at High Metallicity. *Astrophys. J.* **890**, 113, DOI: [10.3847/1538-4357/ab6d77](https://doi.org/10.3847/1538-4357/ab6d77) (2020). [1911.12357](https://arxiv.org/abs/1911.12357).
24. Vink, J. S. Theory and Diagnostics of Hot Star Mass Loss. *arXiv e-prints* arXiv:2109.08164 (2021). [2109.08164](https://arxiv.org/abs/2109.08164).
25. Chiosi, C. & Maeder, A. The evolution of massive stars with mass loss. *Annu. Rev. Astron. Astrophys.* **24**, 329–375, DOI: [10.1146/annurev.aa.24.090186.001553](https://doi.org/10.1146/annurev.aa.24.090186.001553) (1986).
26. Maeder, A. & Meynet, G. Grids of evolutionary models of massive stars with mass loss and overshooting - Properties of Wolf-Rayet stars sensitive to overshooting. *Astron. Astrophys.* **182**, 243–263 (1987).
27. Hurley, J. R., Tout, C. A. & Pols, O. R. Evolution of binary stars and the effect of tides on binary populations. *Mon. Not. R. Astron. Soc.* **329**, 897–928, DOI: [10.1046/j.1365-8711.2002.05038.x](https://doi.org/10.1046/j.1365-8711.2002.05038.x) (2002). [astro-ph/0201220](https://arxiv.org/abs/astro-ph/0201220).
28. Breivik, K. *et al.* COSMIC Variance in Binary Population Synthesis. *Astrophys. J.* **898**, 71, DOI: [10.3847/1538-4357/ab9d85](https://doi.org/10.3847/1538-4357/ab9d85) (2020). [1911.00903](https://arxiv.org/abs/1911.00903).
29. Riley, J. *et al.* Rapid Stellar and Binary Population Synthesis with COMPAS. *Astrophys. J. Suppl. Ser.* **258**, 34, DOI: [10.3847/1538-4365/ac416c](https://doi.org/10.3847/1538-4365/ac416c) (2022). [2109.10352](https://arxiv.org/abs/2109.10352).
30. Izzard, R. G., Tout, C. A., Karakas, A. I. & Pols, O. R. A new synthetic model for asymptotic giant branch stars. *Mon. Not. R. Astron. Soc.* **350**, 407–426, DOI: [10.1111/j.1365-2966.2004.07446.x](https://doi.org/10.1111/j.1365-2966.2004.07446.x) (2004). [astro-ph/0402403](https://arxiv.org/abs/astro-ph/0402403).
31. Izzard, R. G., Dray, L. M., Karakas, A. I., Lugaro, M. & Tout, C. A. Population nucleosynthesis in single and binary stars. I. Model. *Astron. Astrophys.* **460**, 565–572, DOI: [10.1051/0004-6361:20066129](https://doi.org/10.1051/0004-6361:20066129) (2006).
32. Izzard, R. G., Glebbeek, E., Stancliffe, R. J. & Pols, O. R. Population synthesis of binary carbon-enhanced metal-poor stars. *Astron. Astrophys.* **508**, 1359–1374, DOI: [10.1051/0004-6361/200912827](https://doi.org/10.1051/0004-6361/200912827) (2009). [0910.2158](https://arxiv.org/abs/0910.2158).

33. Giacobbo, N., Mapelli, M. & Spera, M. Merging black hole binaries: the effects of progenitor's metallicity, mass-loss rate and Eddington factor. *Mon. Not. R. Astron. Soc.* **474**, 2959–2974, DOI: [10.1093/mnras/stx2933](https://doi.org/10.1093/mnras/stx2933) (2018). [1711.03556](https://arxiv.org/abs/1711.03556).
34. Belczynski, K., Kalogera, V. & Bulik, T. A Comprehensive Study of Binary Compact Objects as Gravitational Wave Sources: Evolutionary Channels, Rates, and Physical Properties. *Astrophys. J.* **572**, 407–431, DOI: [10.1086/340304](https://doi.org/10.1086/340304) (2002). [astro-ph/0111452](https://arxiv.org/abs/astro-ph/0111452).
35. Hurley, J. R., Pols, O. R. & Tout, C. A. Comprehensive analytic formulae for stellar evolution as a function of mass and metallicity. *Mon. Not. R. Astron. Soc.* **315**, 543–569, DOI: [10.1046/j.1365-8711.2000.03426.x](https://doi.org/10.1046/j.1365-8711.2000.03426.x) (2000). [astro-ph/0001295](https://arxiv.org/abs/astro-ph/0001295).
36. Pols, O. R., Schröder, K.-P., Hurley, J. R., Tout, C. A. & Eggleton, P. P. Stellar evolution models for $Z = 0.0001$ to 0.03 . *Mon. Not. R. Astron. Soc.* **298**, 525–536, DOI: [10.1046/j.1365-8711.1998.01658.x](https://doi.org/10.1046/j.1365-8711.1998.01658.x) (1998).
37. Agrawal, P., Hurley, J., Stevenson, S., Szécsi, D. & Flynn, C. The fates of massive stars: exploring uncertainties in stellar evolution with METISSE. *Mon. Not. R. Astron. Soc.* **497**, 4549–4564, DOI: [10.1093/mnras/staa2264](https://doi.org/10.1093/mnras/staa2264) (2020). [2005.13177](https://arxiv.org/abs/2005.13177).
38. Romagnolo, A. *et al.* The role of stellar expansion on the formation of gravitational wave sources. *arXiv e-prints* arXiv:2211.15800 (2022). [2211.15800](https://arxiv.org/abs/2211.15800).
39. Paxton, B. *et al.* Modules for Experiments in Stellar Astrophysics (MESA): Binaries, Pulsations, and Explosions. *Astrophys. J. Suppl. Ser.* **220**, 15, DOI: [10.1088/0067-0049/220/1/15](https://doi.org/10.1088/0067-0049/220/1/15) (2015). [1506.03146](https://arxiv.org/abs/1506.03146).
40. Fragos, T. *et al.* POSYDON: A General-Purpose Population Synthesis Code with Detailed Binary-Evolution Simulations. *arXiv e-prints* arXiv:2202.05892 (2022). [2202.05892](https://arxiv.org/abs/2202.05892).
41. Paxton, B. *et al.* Modules for Experiments in Stellar Astrophysics (MESA). *Astrophys. J. Suppl. Ser.* **192**, 3, DOI: [10.1088/0067-0049/192/1/3](https://doi.org/10.1088/0067-0049/192/1/3) (2011). [1009.1622](https://arxiv.org/abs/1009.1622).
42. Paxton, B. *et al.* Modules for Experiments in Stellar Astrophysics (MESA): Planets, Oscillations, Rotation, and Massive Stars. *Astrophys. J. Suppl. Ser.* **208**, 4, DOI: [10.1088/0067-0049/208/1/4](https://doi.org/10.1088/0067-0049/208/1/4) (2013). [1301.0319](https://arxiv.org/abs/1301.0319).
43. Paxton, B. *et al.* Modules for Experiments in Stellar Astrophysics (MESA): Convective Boundaries, Element Diffusion, and Massive Star Explosions. *Astrophys. J. Suppl. Ser.* **234**, 34, DOI: [10.3847/1538-4365/aaa5a8](https://doi.org/10.3847/1538-4365/aaa5a8) (2018). [1710.08424](https://arxiv.org/abs/1710.08424).
44. Paxton, B. *et al.* Modules for Experiments in Stellar Astrophysics (MESA): Pulsating Variable Stars, Rotation, Convective Boundaries, and Energy Conservation. *Astrophys. J. Suppl. Ser.* **243**, 10, DOI: [10.3847/1538-4365/ab2241](https://doi.org/10.3847/1538-4365/ab2241) (2019). [1903.01426](https://arxiv.org/abs/1903.01426).
45. Kruckow, M. U., Tauris, T. M., Langer, N., Kramer, M. & Izzard, R. G. Progenitors of gravitational wave mergers: binary evolution with the stellar grid-based code COMBINE. *Mon. Not. R. Astron. Soc.* **481**, 1908–1949, DOI: [10.1093/mnras/sty2190](https://doi.org/10.1093/mnras/sty2190) (2018). [1801.05433](https://arxiv.org/abs/1801.05433).
46. Eldridge, J. J. *et al.* Binary Population and Spectral Synthesis Version 2.1: Construction, Observational Verification, and New Results. *Publ. Astron. Soc. Aust.* **34**, e058, DOI: [10.1017/pasa.2017.51](https://doi.org/10.1017/pasa.2017.51) (2017). [1710.02154](https://arxiv.org/abs/1710.02154).
47. Stancliffe, R. J. & Eldridge, J. J. Modelling the binary progenitor of Supernova 1993J. *Mon. Not. R. Astron. Soc.* **396**, 1699–1708, DOI: [10.1111/j.1365-2966.2009.14849.x](https://doi.org/10.1111/j.1365-2966.2009.14849.x) (2009). [0904.0282](https://arxiv.org/abs/0904.0282).
48. Dominik, M. *et al.* Double Compact Objects. II. Cosmological Merger Rates. *Astrophys. J.* **779**, 72, DOI: [10.1088/0004-637X/779/1/72](https://doi.org/10.1088/0004-637X/779/1/72) (2013). [1308.1546](https://arxiv.org/abs/1308.1546).
49. Neijssel, C. J. *et al.* The effect of the metallicity-specific star formation history on double compact object mergers. *Mon. Not. R. Astron. Soc.* **490**, 3740–3759, DOI: [10.1093/mnras/stz2840](https://doi.org/10.1093/mnras/stz2840) (2019). [1906.08136](https://arxiv.org/abs/1906.08136).
50. Broekgaarden, F. S. *et al.* Impact of massive binary star and cosmic evolution on gravitational wave observations - II. Double compact object rates and properties. *Mon. Not. R. Astron. Soc.* **516**, 5737–5761, DOI: [10.1093/mnras/stac1677](https://doi.org/10.1093/mnras/stac1677) (2022). [2112.05763](https://arxiv.org/abs/2112.05763).
51. Meynet, G. & Maeder, A. Stellar evolution with rotation. X. Wolf-Rayet star populations at solar metallicity. *Astron. Astrophys.* **404**, 975–990, DOI: [10.1051/0004-6361:20030512](https://doi.org/10.1051/0004-6361:20030512) (2003). [astro-ph/0304069](https://arxiv.org/abs/astro-ph/0304069).
52. Ekström, S. *et al.* Grids of stellar models with rotation. I. Models from 0.8 to $120 M_{\odot}$ at solar metallicity ($Z = 0.014$). *Astron. Astrophys.* **537**, A146, DOI: [10.1051/0004-6361/201117751](https://doi.org/10.1051/0004-6361/201117751) (2012). [1110.5049](https://arxiv.org/abs/1110.5049).
53. Choi, J. *et al.* Mesa Isochrones and Stellar Tracks (MIST). I. Solar-scaled Models. *Astrophys. J.* **823**, 102, DOI: [10.3847/0004-637X/823/2/102](https://doi.org/10.3847/0004-637X/823/2/102) (2016). [1604.08592](https://arxiv.org/abs/1604.08592).
54. Smith, N. Luminous blue variables and the fates of very massive stars. *Philos. Transactions Royal Soc. Lond. Ser. A* **375**, 20160268, DOI: [10.1098/rsta.2016.0268](https://doi.org/10.1098/rsta.2016.0268) (2017).

55. Patton, R. A. & Sukhbold, T. Towards a realistic explosion landscape for binary population synthesis. *Mon. Not. R. Astron. Soc.* **499**, 2803–2816, DOI: [10.1093/mnras/staa3029](https://doi.org/10.1093/mnras/staa3029) (2020). [2005.03055](https://arxiv.org/abs/2005.03055).
56. Fryer, C. L. *et al.* Compact Remnant Mass Function: Dependence on the Explosion Mechanism and Metallicity. *Astrophys. J.* **749**, 91, DOI: [10.1088/0004-637X/749/1/91](https://doi.org/10.1088/0004-637X/749/1/91) (2012). [1110.1726](https://arxiv.org/abs/1110.1726).
57. Dorozsmai, A. & Toonen, S. Importance of stable mass transfer and stellar winds for the formation of gravitational wave sources. *arXiv e-prints* arXiv:2207.08837 (2022). [2207.08837](https://arxiv.org/abs/2207.08837).
58. Aasi, J. *et al.* Advanced LIGO. *Class. Quantum Gravity* **32**, 074001, DOI: [10.1088/0264-9381/32/7/074001](https://doi.org/10.1088/0264-9381/32/7/074001) (2015). [1411.4547](https://arxiv.org/abs/1411.4547).
59. Bavera, S. S. *et al.* Probing the progenitors of spinning binary black-hole mergers with long gamma-ray bursts. *Astron. Astrophys.* **657**, L8, DOI: [10.1051/0004-6361/202141979](https://doi.org/10.1051/0004-6361/202141979) (2022). [2106.15841](https://arxiv.org/abs/2106.15841).
60. van den Heuvel, E. P. J., Portegies Zwart, S. F. & de Mink, S. E. Forming short-period Wolf-Rayet X-ray binaries and double black holes through stable mass transfer. *Mon. Not. R. Astron. Soc.* **471**, 4256–4264, DOI: [10.1093/mnras/stx1430](https://doi.org/10.1093/mnras/stx1430) (2017). [1701.02355](https://arxiv.org/abs/1701.02355).
61. Pavlovskii, K., Ivanova, N., Belczynski, K. & Van, K. X. Stability of mass transfer from massive giants: double black hole binary formation and ultraluminous X-ray sources. *Mon. Not. R. Astron. Soc.* **465**, 2092–2100, DOI: [10.1093/mnras/stw2786](https://doi.org/10.1093/mnras/stw2786) (2017). [1606.04921](https://arxiv.org/abs/1606.04921).
62. Kalogera, V., Belczynski, K., Kim, C., O’Shaughnessy, R. & Willems, B. Formation of double compact objects. *Phys. Rep.* **442**, 75–108, DOI: [10.1016/j.physrep.2007.02.008](https://doi.org/10.1016/j.physrep.2007.02.008) (2007). [astro-ph/0612144](https://arxiv.org/abs/astro-ph/0612144).
63. Bavera, S. S. *et al.* The origin of spin in binary black holes. Predicting the distributions of the main observables of Advanced LIGO. *Astron. Astrophys.* **635**, A97, DOI: [10.1051/0004-6361/201936204](https://doi.org/10.1051/0004-6361/201936204) (2020). [1906.12257](https://arxiv.org/abs/1906.12257).
64. Bavera, S. S. *et al.* The impact of mass-transfer physics on the observable properties of field binary black hole populations. *Astron. Astrophys.* **647**, A153, DOI: [10.1051/0004-6361/202039804](https://doi.org/10.1051/0004-6361/202039804) (2021). [2010.16333](https://arxiv.org/abs/2010.16333).
65. Nelson, D. *et al.* The illustris simulation: Public data release. *Astron. Comput.* **13**, 12–37, DOI: [10.1016/j.ascom.2015.09.003](https://doi.org/10.1016/j.ascom.2015.09.003) (2015). [1504.00362](https://arxiv.org/abs/1504.00362).
66. Abbott, B. P. *et al.* Prospects for observing and localizing gravitational-wave transients with Advanced LIGO, Advanced Virgo and KAGRA. *Living Rev. Relativ.* **21**, 3, DOI: [10.1007/s41114-018-0012-9](https://doi.org/10.1007/s41114-018-0012-9) (2018). [1304.0670](https://arxiv.org/abs/1304.0670).
67. Abbott, R. *et al.* The population of merging compact binaries inferred using gravitational waves through GWTC-3. *arXiv e-prints* arXiv:2111.03634 (2021). [2111.03634](https://arxiv.org/abs/2111.03634).
68. Fragos, T. & McClintock, J. E. The Origin of Black Hole Spin in Galactic Low-mass X-Ray Binaries. *Astrophys. J.* **800**, 17, DOI: [10.1088/0004-637X/800/1/17](https://doi.org/10.1088/0004-637X/800/1/17) (2015). [1408.2661](https://arxiv.org/abs/1408.2661).
69. Qin, Y. *et al.* The spin of the second-born black hole in coalescing binary black holes. *Astron. Astrophys.* **616**, A28, DOI: [10.1051/0004-6361/201832839](https://doi.org/10.1051/0004-6361/201832839) (2018). [1802.05738](https://arxiv.org/abs/1802.05738).
70. Bavera, S. S., Zevin, M. & Fragos, T. Approximations of the Spin of Close Black Hole-Wolf-Rayet Binaries. *Res. Notes Am. Astron. Soc.* **5**, 127, DOI: [10.3847/2515-5172/ac053c](https://doi.org/10.3847/2515-5172/ac053c) (2021). [2105.09077](https://arxiv.org/abs/2105.09077).
71. Graham, J. F., Schady, P. & Fruchter, A. S. A Surprising Lack of LGRB Metallicity Evolution with Redshift. *arXiv e-prints* arXiv:1904.02673 (2019). [1904.02673](https://arxiv.org/abs/1904.02673).
72. Spera, M. *et al.* Merging black hole binaries with the SEVN code. *Mon. Not. R. Astron. Soc.* **485**, 889–907, DOI: [10.1093/mnras/stz359](https://doi.org/10.1093/mnras/stz359) (2019). [1809.04605](https://arxiv.org/abs/1809.04605).
73. Iorio, G. *et al.* Compact object mergers: exploring uncertainties from stellar and binary evolution with SEVN. *arXiv e-prints* arXiv:2211.11774 (2022). [2211.11774](https://arxiv.org/abs/2211.11774).
74. Kruckow, M. U. *Binary star population synthesis - Progenitors of gravitational wave driven mergers*. Ph.D. thesis, Rheinische Friedrich Wilhelms University of Bonn, Germany (2018).
75. Eldridge, J. J. & Stanway, E. R. BPASS predictions for binary black hole mergers. *Mon. Not. R. Astron. Soc.* **462**, 3302–3313, DOI: [10.1093/mnras/stw1772](https://doi.org/10.1093/mnras/stw1772) (2016). [1602.03790](https://arxiv.org/abs/1602.03790).
76. Farr, W. M. *et al.* Distinguishing spin-aligned and isotropic black hole populations with gravitational waves. *Nature* **548**, 426–429, DOI: [10.1038/nature23453](https://doi.org/10.1038/nature23453) (2017). [1706.01385](https://arxiv.org/abs/1706.01385).
77. Misra, D. *et al.* X-ray luminosity function of high-mass X-ray binaries: Studying the signatures of different physical processes using detailed binary evolution calculations. *arXiv e-prints* arXiv:2209.05505 (2022). [2209.05505](https://arxiv.org/abs/2209.05505).

78. Rout, S. K., Vadawale, S., Garcia, J. & Connors, R. Revisiting the galactic X-ray binary MAXI J1631-479: Implications for high inclination and a massive black hole. *arXiv e-prints* arXiv:2212.05293 (2022). [2212.05293](#).
79. Thompson, T. A. *et al.* A noninteracting low-mass black hole-giant star binary system. *Science* **366**, 637–640, DOI: [10.1126/science.aau4005](#) (2019). [1806.02751](#).
80. Jayasinghe, T. *et al.* A unicorn in monoceros: the 3 M_{\odot} dark companion to the bright, nearby red giant V723 Mon is a non-interacting, mass-gap black hole candidate. *Mon. Not. R. Astron. Soc.* **504**, 2577–2602, DOI: [10.1093/mnras/stab907](#) (2021). [2101.02212](#).
81. Giesers, B. *et al.* A stellar census in globular clusters with MUSE: Binaries in NGC 3201. *Astron. Astrophys.* **632**, A3, DOI: [10.1051/0004-6361/201936203](#) (2019). [1909.04050](#).
82. Saracino, S. *et al.* A black hole detected in the young massive LMC cluster NGC 1850. *Mon. Not. R. Astron. Soc.* **511**, 2914–2924, DOI: [10.1093/mnras/stab3159](#) (2022). [2111.06506](#).
83. Breivik, K., Chatterjee, S. & Larson, S. L. Revealing Black Holes with Gaia. *Astrophys. J. Lett.* **850**, L13, DOI: [10.3847/2041-8213/aa97d5](#) (2017). [1710.04657](#).
84. Chawla, C. *et al.* Gaia May Detect Hundreds of Well-characterised Stellar Black Holes. *arXiv e-prints* arXiv:2110.05979 (2021). [2110.05979](#).
85. Callister, T. A., Miller, S. J., Chatziioannou, K. & Farr, W. M. No Evidence that the Majority of Black Holes in Binaries Have Zero Spin. *Astrophys. J. Lett.* **937**, L13, DOI: [10.3847/2041-8213/ac847e](#) (2022). [2205.08574](#).
86. Humphreys, R. M. & Davidson, K. The Luminous Blue Variables: Astrophysical Geysers. *Publ. Astron. Soc. Pac.* **106**, 1025, DOI: [10.1086/133478](#) (1994).
87. Barrett, J. W. *et al.* Accuracy of inference on the physics of binary evolution from gravitational-wave observations. *Mon. Not. R. Astron. Soc.* **477**, 4685–4695, DOI: [10.1093/mnras/sty908](#) (2018). [1711.06287](#).
88. Ng, K. K. Y. *et al.* Gravitational-wave astrophysics with effective-spin measurements: Asymmetries and selection biases. *Phys. Rev. D* **98**, 083007, DOI: [10.1103/PhysRevD.98.083007](#) (2018). [1805.03046](#).
89. LIGO Scientific Collaboration. LIGO Algorithm Library - LALSuite. free software (GPL), DOI: [10.7935/GT1W-FZ16](#) (2018).
90. Finn, L. S. & Chernoff, D. F. Observing binary inspiral in gravitational radiation: One interferometer. *Phys. Rev. D* **47**, 2198–2219, DOI: [10.1103/PhysRevD.47.2198](#) (1993). [gr-qc/9301003](#).
91. Aasi, J. *et al.* Search of the Orion spur for continuous gravitational waves using a loosely coherent algorithm on data from LIGO interferometers. *Phys. Rev. D* **93**, 042006, DOI: [10.1103/PhysRevD.93.042006](#) (2016). [1510.03474](#).
92. Hunter, J. D. Matplotlib: A 2d graphics environment. *Comput. Sci. & Eng.* **9**, 90–95, DOI: [10.1109/MCSE.2007.55](#) (2007).
93. Price-Whelan, A. M. *et al.* The astropy project: Building an open-science project and status of the v2. 0 core package. *The Astron. J.* **156**, 123 (2018).
94. Pérez, F. & Granger, B. E. IPython: a system for interactive scientific computing. *Comput. Sci. Eng.* **9**, 21–29, DOI: [10.1109/MCSE.2007.53](#) (2007).
95. Harris, C. R. *et al.* Array programming with NumPy. *Nature* **585**, 357–362, DOI: [10.1038/s41586-020-2649-2](#) (2020).
96. The pandas development team. pandas-dev/pandas: Pandas, DOI: [10.5281/zenodo.7344967](#) (2022).
97. Virtanen, P. *et al.* SciPy 1.0: Fundamental Algorithms for Scientific Computing in Python. *Nat. Methods* **17**, 261–272, DOI: [10.1038/s41592-019-0686-2](#) (2020).

Supplementary information

A No stellar wind model variation

We consider an illustrative model variation where there is no mass loss due to stellar winds. Figure 5 shows the stellar evolutionary tracks of such model showing the surface ^1H and centre ^4He abundances of the stars during their evolution. Similar to the constant-mass stellar tracks implemented in SSE,³⁵ we find that independently of their ZAMS mass, these massive stars expand to become red-supergiant stars with radii of $\sim 1000R_\odot$. This exercise shows the importance of self-consistently modeling stellar-wind mass loss in stellar evolution. Failing to do so leads to miscalculation of the structure resulting in bigger cores, altered surface chemistry, and nonphysical binary interactions with important implications for BBH formation.

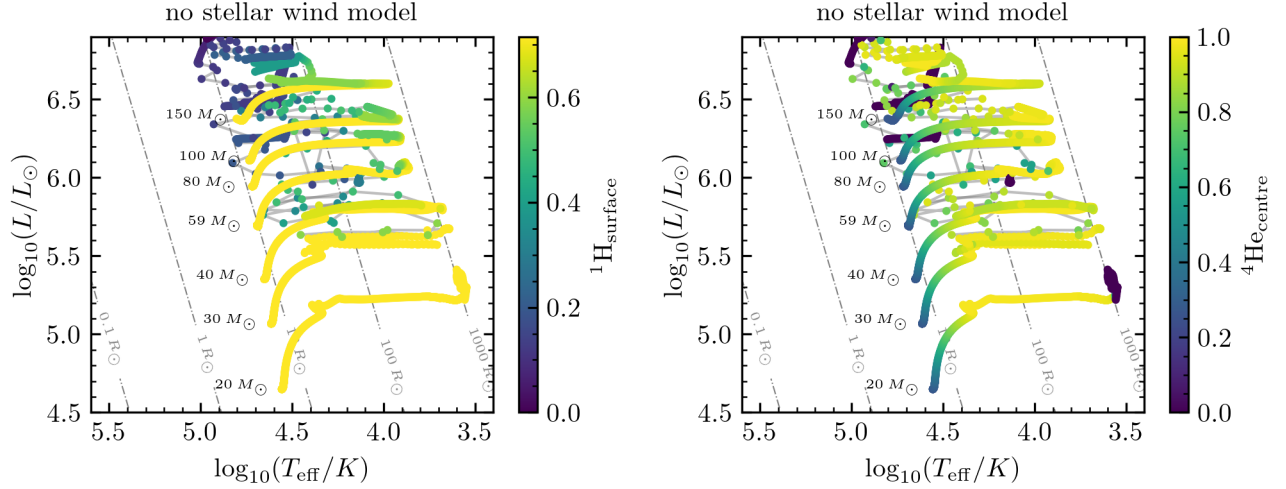


Figure 5. Hertzsprung–Russell diagram for stars with masses between $20M_\odot$ and $150M_\odot$. We show a variation of our stellar models without any stellar wind mass loss. The instantaneous surface hydrogen abundance (*left*) and centre helium abundance (*right*) are colour-coded in the tracks. In contrast to the default model, we find that not accounting for the stellar wind feedback onto stellar evolution in the stellar models cause massive stars ($\gtrsim 50M_\odot$) to expand up to $\sim 1000R_\odot$.

B The origin of spin in first-born black holes

In Figure 6, we provide two two-dimensional slices of the MESA binary grid of POSYDON consisting of two stars initially at ZAMS. We show our simulation outcomes as a function of initial primary star mass M_1 and orbital period P_{orb} for a fixed mass ratio $q \equiv M_2/M_1$, where M_2 is the secondary initial star mass. In the left panel we show one example of a mass ratio $q = 0.4$, and on the right a more-equal mass ratio $q = 0.9$ slice. Each point in the panels represents a separate MESA binary simulation from our grid where different markers shapes and colors distinguish different binary evolution phases prior to the formation of the first-born compact object. An exception to this are triangular markers which are overlaid onto the grid and represent binary systems from our fiducial POSYDON population synthesis study, which will evolve to become a merging BBH. These systems are the subsample of merging BBHs with ZAMS mass ratios corresponding to the mass ratios of 0.4 ± 0.025 and 0.9 ± 0.025 , respectively. The colour of these triangular markers indicate the spin of the first-born BH. We distinguish binaries that will later evolve through a stable mass-transfer phase from the ones that later evolve through a common-envelope phase; the latter are only present in the mass ratio slice of $q = 0.4$. At the bottom of the left panel, at short orbital periods and for massive stars $M_1 \gtrsim 60M_\odot$, we see binaries that either undergo a stable mass transfer, a contact stable phase or, alternatively avoided any mass transfer phase and formed mildly spinning first-born BHs ($\chi_{\text{BH1}} \leq 0.2$). Figure 6 shows that this evolution would not be possible at similar initial orbital periods and smaller primary masses as the increased maximal expansion of these stars would lead to unstable mass transfer, followed by a stellar merger. Finally, this evolutionary pathway is not present at more-equal mass ratios because the more massive stellar companion would not expand to become a supergiant star to initiate a mass transfer episode after the formation of the first-born BH.

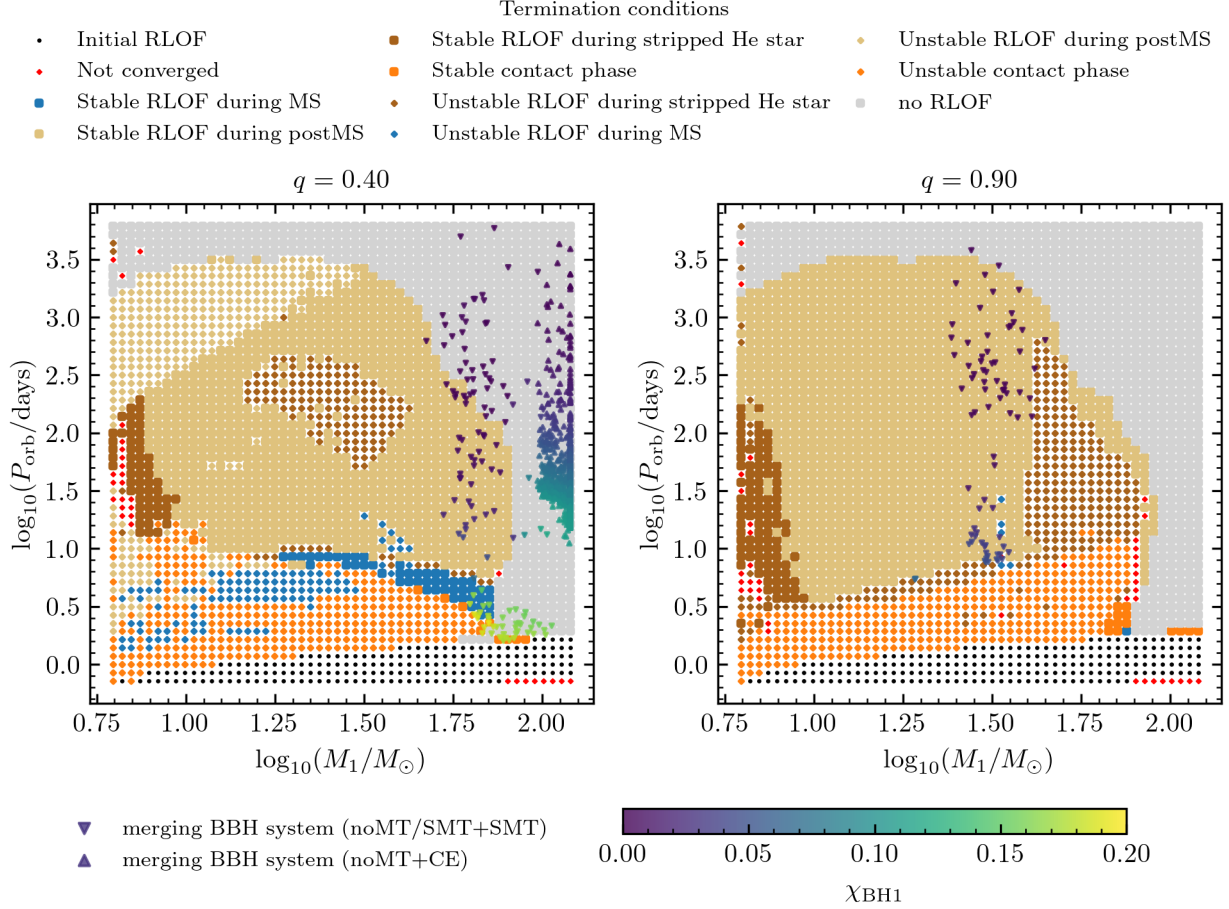


Figure 6. View of two MESA grid slices, for two different values of initial binary mass ratio ($q = 0.4$ on the left, $q = 0.9$ on the right), from our MESA grid of binary-star models consisting of two stars, initially at ZAMS. The different symbols summarize the evolution of each of the models. We distinguish between models that experienced stable and no mass transfer (squares), which reach the end of the life of the primary stars, and the ones that stopped during mass transfer due to dynamical instability (diamonds). Different colors distinguish the evolutionary phase of the donor star during the latest episode of mass transfer. We also indicate systems that were in initial Roche-lobe overflow (RLOF) at birth and those that stopped prematurely for numerical reasons. Finally, we overlay with triangle markers binary systems of the POSYDON population synthesis model that further evolve to merging BBHs distinguishing systems that later evolve through an additional stable mass transfer (SMT) or common envelope (CE) according to the legend. The colors of these markers indicate the spin magnitude of the first-born BH according to the colorbar. We see most of mildly spinning BHs to originate in the part of the parameter space of massive primary stars and low initial orbital separations in the mass ratio slice $q = 0.4$.